25th ABCM International Congress of Mechanical Engineering
October 20-25, 2019, Uberlândia, MG, Brazil

COB-2019-0600
DEVELOPMENT OF A SYSTEM FOR THE CHARACTERIZATION OF SMALL VERTICAL AXIS WIND TURBINES

Gunther Damaceno Barbosa
Mozart Azevedo Portilho Pinheiro
Julio Carlos Teixeira
João Vicente Akwa
Centro de Engenharia, Modelagem e Ciências Sociais Aplicadas, Universidade Federal do ABC, Brazil
gunther.b@ufabc.edu.br; mozart.portilho@aluno.ufabc.edu.br; juliocarlos.teixeira@ufabc.edu.br; joao.akwa@ufabc.edu.br

Abstract. *In this work, a small aerodynamic channel was developed to test reduced models of vertical axis wind turbines. A model of the Savonius turbine was built in 3D printer and had its torque and power measured during operation at varying wind and angular velocities. For measurements, a Foucault brake and a device for torque measurement were also developed. The maximum power coefficient C_P obtained after the blockage effect correction is 0.107, which occurs in tip speed ratio 0.707. At the optimum performance point, the torque coefficient C_T is 0.152, while the maximum torque coefficient is 0.217 in the tip speed ratio 0.354. The obtained results are in accordance with the ranges of values obtained in other studies for this type of device. The system can be used in the future to test different configurations of small vertical wind turbines with low cost and space saving.*

Keywords: *aerodynamic channel; Savonius turbine; measurements; operation; performance curves.*

1. INTRODUCTION

In the current Brazilian energy scenario, the number of decentralized energy generation systems is increasing. The use of small vertical axis turbines, such as the Savonius turbine, could be a solution for power generation in urban and rural areas at low cost. This type of turbine, which works mainly due to the drag forces of pressure in its buckets, has low cost and is easy to build among the main advantages of its use. The power coefficient of Savonius is usually lower than that achieved by turbines such as the horizontal axis turbine, as well as the Darrieus vertical axis one, which are based on lifting forces. However, if improvement studies could be carried out to increase the performance of a Savonius wind turbine, its use could be favored due to its lower manufacturing cost (Savonius, 1930; Vance, 1973; Fujisawa, 1992; Menet, 2004; Kamoji et al., 2008; Saha et al., 2008; Kumar et al., 2018).

In view of the importance and utility that small wind turbines may have on the current context, this work aimed at developing a test system for small-scale vertical axis wind turbines. The system was developed by the Renewable Energy Laboratory of the Universidade Federal do ABC (UFABC). In the system design, a closed-section open circuit aerodynamic channel was constructed and used to test a reduced model of a vertical Savonius wind turbine. The turbine model was made with acrylonitrile butadiene styrene (ABS) using the 3D printing technique. In the present research work, the turbine was evaluated under operating conditions, submitted to different loads, with angular velocities, torque and power measurements. Parallel studies on turbine operation without the aerodynamic channel blockage effect are being developed in the laboratory using computational fluid dynamics validation tests and flow analysis. Thus, the system can be used in the future to test different configurations of wind turbines with low cost and space saving.

2. METHODOLOGY

The aerodynamic channel assembly was performed according to Fig. 1, with air being released by a blower through a diffuser, to a series of classic homogenizers (grid type, honeycomb and fine grid). After the homogenizers, the air goes to the test section with 0.146 m height by 0.193 m width, positioned 0.5 m from the fine grid homogenizer. A Pitot tube positioned upstream from the test section can measure the air velocity. A frequency inverter that controls the blower rotation is used to vary the wind velocity. These dimensions were chosen to have flow conditions close to those obtained by Akwa (2014), who studied the flow in a Savonius rotor under static conditions, with a turbulence intensity in the order of 1% downstream from homogenizers.

The turbine operation was tested using an acrylonitrile butadiene styrene (ABS) device built by a 3D printer and can be visualized in Fig. 2. This turbine has no passing shaft. The turbine was designed to have a diameter d equal to 0.05 m,

with two semicircular profile buckets with 0.002 m thickness. The buckets overlapping *s* is 0.006 m in length, as shown in Fig. 2-b. Thus, the ratio of overlapping buckets calculated as *s*/*c*, where *c* is the bucket cord according to Akwa et al. (2012a), is equal to 0.214. This value is slightly higher than the ideal obtained value of 0.15 because the buckets have a relatively large thickness for this turbine size and an increase in overlapping allows a greater amount of air to be deflected to the bucket, whose movement is contrary to the main direction of the flow, increasing the performance of the turbine (Akwa et al., 2012a; Akwa et al., 2012b). During the experiments, the turbine was fixed so that the upper and lower tips were accessible from the outer side of the aerodynamic channel, in which torque and angular velocity measurements were performed. This form of fixation was also used to reduce the tip losses effects on the turbine operation, which were not evaluated in this work. The turbine fixation could be done thanks to openings made by laser cuts, thus, the test of other vertical turbines in the channel can be performed only with the rotor replacement.

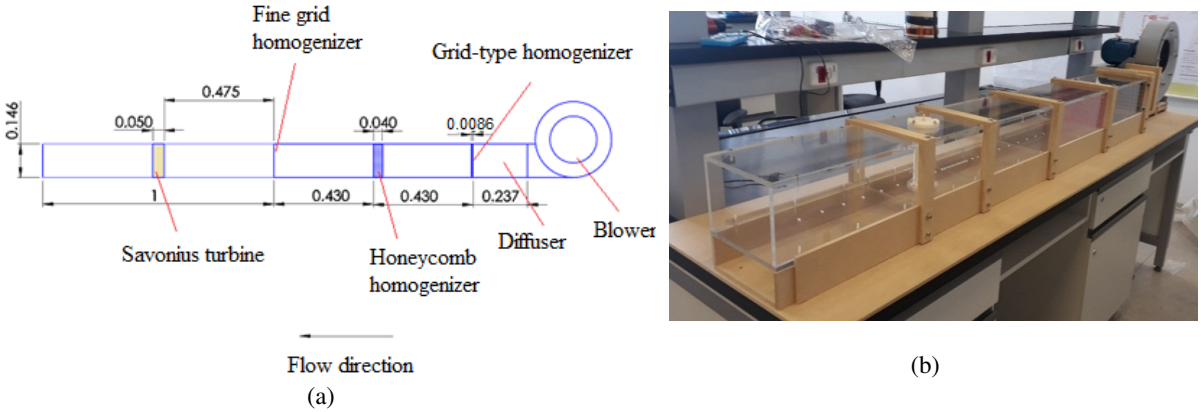

Figure 1 – Aerodynamic channel: (a) schematic diagram (dimensions in meters); (b) assembly photography.

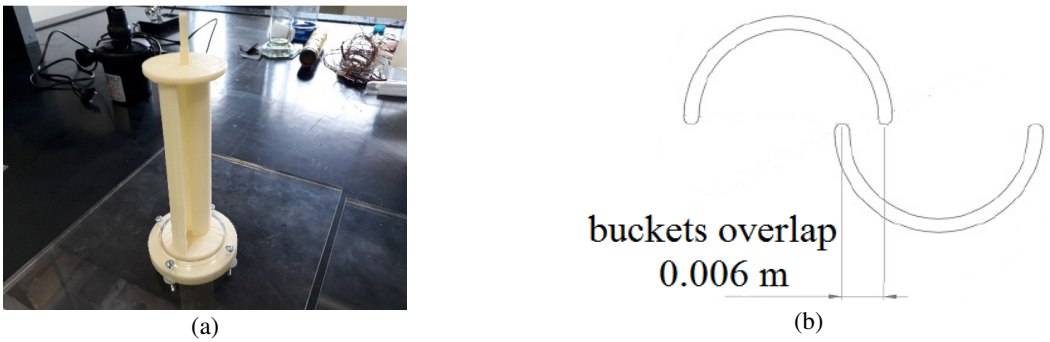

Figure 2 – Wind turbine: (a) turbine photography; (b) drawing of the rotor configuration profile.

To perform the tests, a device consisting of eddy current brake and sensor for dynamic torque measurement was developed, as shown in Fig. 3. The eddy current brake was used to vary the load on the turbine shaft, while the sensor of torque captured the average torque produced by the turbine. The brake consists of an aluminum disc with 6 cm in diameter and 1 mm thickness connected to the upper tip of the turbine shaft and a neodymium magnet of cylindrical shape with 1 cm in diameter and 0.4 cm in height positioned on the disc, but there is no contact between them. When the turbine is rotating, the disc will also be rotating and, due to the proximity of the magnet, electric currents are induced in the disc, because the material will be subjected to a variable magnetic field. The current induced in the aluminum also generates a magnetic field, consequently causing a force on the magnet. Based on this principle, the magnet was attached to one tip of a rod, while the other tip transfered force to a load cell of an adapted weight balance.

Thus, a force applied on the magnet is transferred to the load cell on the opposite side of the rod. Two methods of transferring the force to the load cell were tested. The first one used the rod as an Archimedes lever, as shown in Fig. 3-a. By using the first method, a bearing was positioned displaced from the center of the rod so that a gain of 2.531 in the force measurement could be obtained. This method was later permanently replaced by the use of the rod connected directly to the load cell, as shown in Fig. 3-b. In the second method, a reduction in the wall thickness of the load cell was made to promote a gain in force measurement equal to 3.795, as shown in Fig. 3-d. Measurements using the rod directly connected to the load cell provided smaller dispersions in the obtained values as shown in Fig. 4 and avoided instabilities of moving parts. In the measurements, the magnet can be approached or distanced from the disc by a set of screws. The greater proximity of the magnet to the disc causes greater braking of the turbine, being used to adjust the turbine's average angular

velocity during torque and power measurements for a given flow velocity. After a calibration process using the rod directly connected to the load cell, the adapted weight balance provided a measure of the useful torque on the turbine shaft, T_{sensor}, given by Eq. (1), where m_b is a value given in grams-force shown on the weight balance screen , C_1 is a coefficient equal to 0.2635 with uncertainty of ±0.0007, R_1 is the force application radius equal to 0.0204 m with uncertainty estimated at ±0.0001 m and g is the local gravity acceleration value, which according to Lopes (2008) can be approximated to 9.7856 m/s². As the m_b resolution is 1 g a gain in force measurement equal to 3.795 (0.2635^{-1}) was used. The calibration was performed using loads with known mass values, previously measured by a weight balance with resolution equal to 0.00001 g. The calibration data are shown in Fig. 5.

$$T_{sensor} = R_1 \cdot \left[\frac{(C_1 \cdot m_b)}{1000}\right] \cdot g = 0.0204 \cdot \left[\frac{(0.2635 \cdot m_b)}{1000}\right] \cdot 9.7856 \quad (1)$$

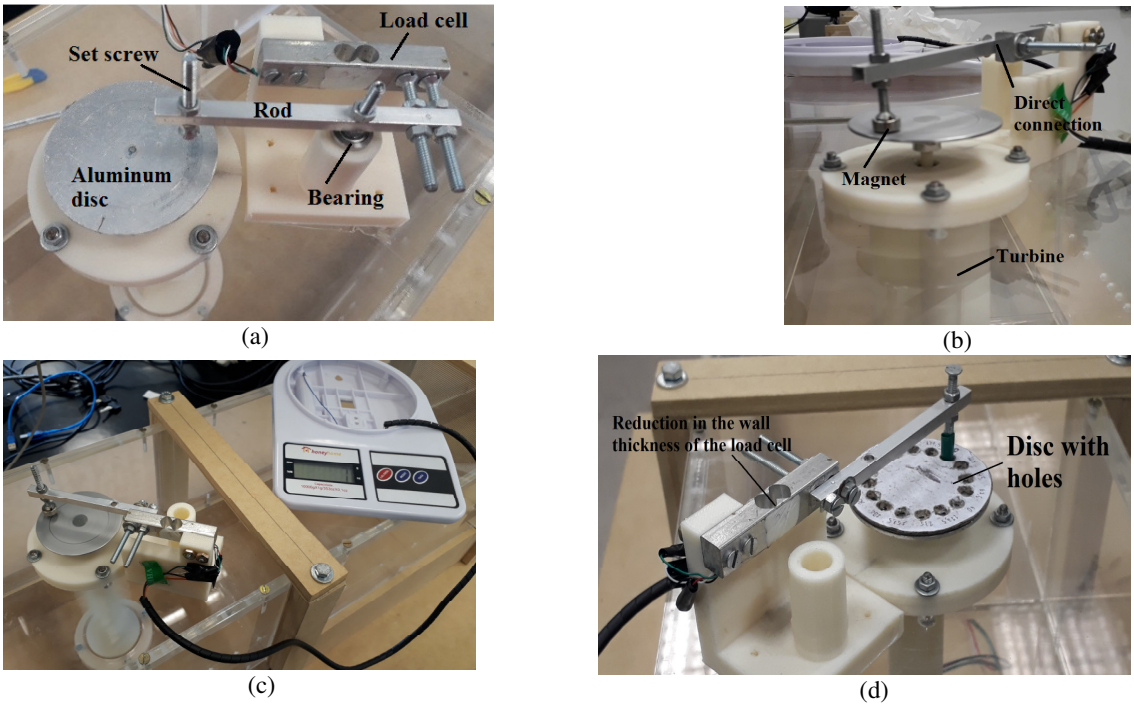

Figure 3 – Foucault brake and sensor for torque measurement: (a) detail of the brake device and load cell using force transfer by Archimedes lever; (b) details of the devices with the rod connected directly to the load cell; (c) reading of the mean value of the m_b (Eq. (1)) by an adapted weight balance; (d) measurement of static torque using a disc with holes.

To measure the static torque, when the angular velocity of the turbine is equal to zero, the magnet is withdrawn and the screw is inserted into the holes of a paper disc, with holes spaced every 22.5° as shown in Fig. 3-d. The static torque can be represented as a function of the angular position of the turbine advance bucket θ and also by a mean value.

The turbine mean values of the angular velocity in each situation were measured by a non-contact meter with a strobe lamp whose measuring principle applies an uncertainty of ±1% of the measured value plus one digit. Thus, the average power in the turbine shaft could be calculated by the product of the average torque in the shaft and the average angular velocity. The power dissipated by friction in the turbine bearings was obtained through an experiment in which the decay of the unloaded turbine rotation was measured with acquisition of the angular velocity values by means of an encoder. To obtain the torque due to friction in the bearings, a hypothesis was used as described by MacPhee and Beyene (2019), who considered the torque due to the friction in the bearings to have a tendency of linear growth with the angular velocity of the turbine. This torque, $T_{bearings\ friction}$, can be obtained by Eq. (2), where τ is the time constant of the turbine deceleration exponential curve, when it is uncharged and decelerates to rest due to friction in the bearings, ω is a turbine angular velocity, J is the moment of inertia of the turbine and other moving parts calculated as 1.8730 x 10^{-5} kg.m^2. τ was obtained from the value of 13.0890 s with an uncertainty of ±0.2399 by measurement the angular velocity in the deceleration of the unloaded turbine by an encoder connected to the lower tip of the turbine shaft and an optical sensor with reading and acquisition of the signals by an arduino. The results of decay of the turbine angular velocity are shown in Fig. 6.

$$T_{bearings\ friction} = \frac{J}{\tau} \cdot \omega \quad (2)$$

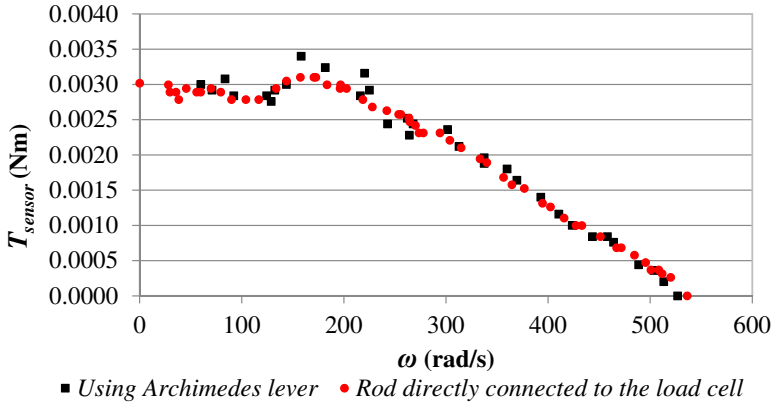

Figure 4 – Comparison between two methods for measuring the useful torque on the turbine shaft T_{sensor} *versus* the angular velocity ω for the blower frequency set at 47 Hz (V_u = 8,98 m/s).

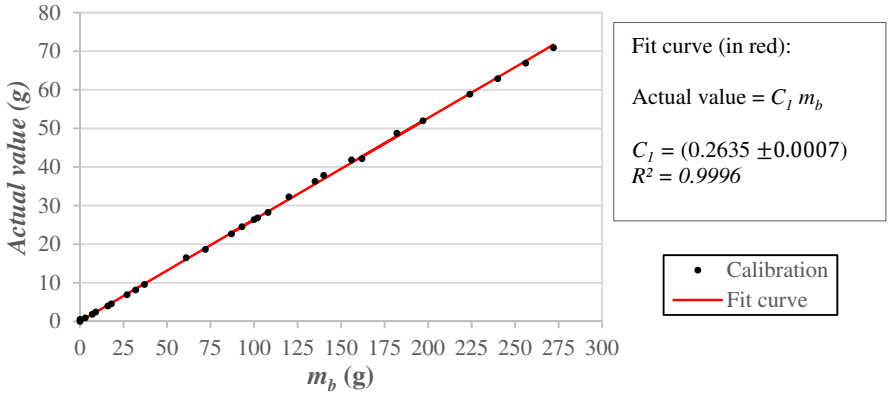

Figure 5 – Load cell calibration data.

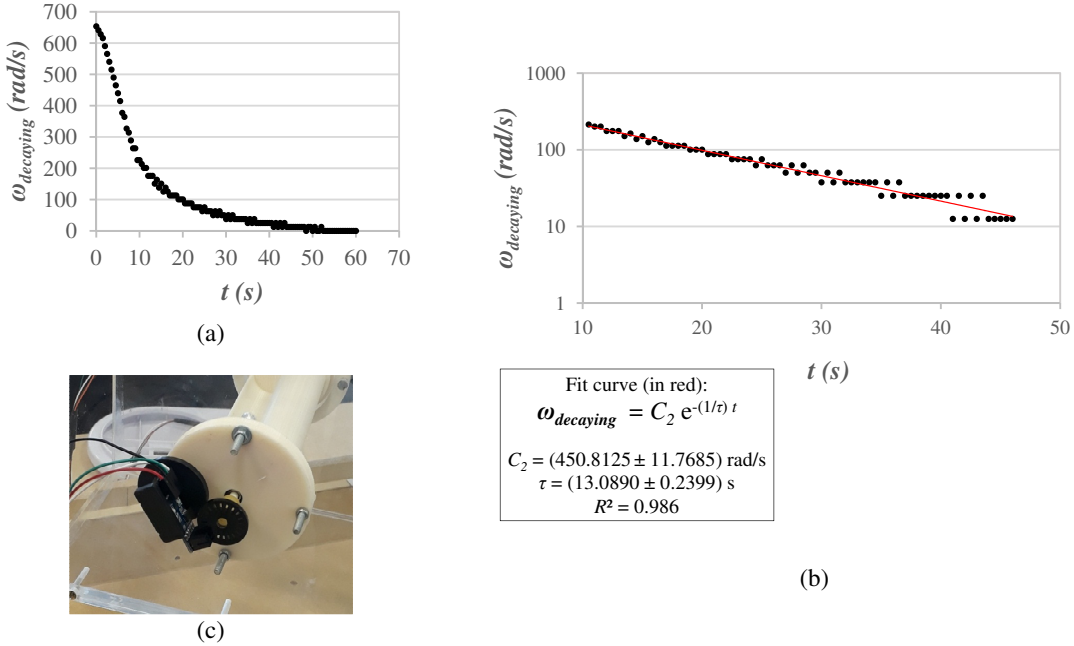

Figure 6 – Decay of angular velocity of the turbine without load on the shaft due to friction in the bearings: (a) in linear scale; (b) in logarithmic scale with adjustment curve; (c) encoder with optical switch.

The power dissipated by friction of the air with the disc of the eddy brake was obtained analytically. The opposite torque due to this friction ($T_{friction\ on\ brake\ disc}$) can be obtained by Eq. (3), resulting from the solution of the three-dimensional flow boundary layer on the upper and lower surfaces of the disc, as explained by Rosa (2009). In the equation, R_{disc} is the maximum radius of the aluminum disc (3 cm), $\tau_{z\theta}$ is the shear stress and ρ and μ are the specific mass and the dynamic viscosity of the air. The specific mass of the air was obtained considering an ideal gas model for the air obtained by Eq. (4) and the viscosity was obtained by the interpolation of the values found in tables of fluid mechanics books using the temperature values as input (Van Wylen et al., 1995; Streeter, 1974; Kothe, 2016). In Equation (4), p_{atm} is the atmospheric pressure and T_{air} is the air temperature. The atmospheric pressure is measured by a barometer with resolution of 100 Pa and a thermometer with resolution of 0.1°C to obtain the air temperature. By using the sum of the three power components, the total average power presented by the turbine P_{total} can be obtained and represented by Eq. (5), where T_{total} is the total torque.

$$T_{friction\ on\ brake\ disc} = 2 \cdot \int_0^{R_{disc}} \tau_{z\theta} \cdot 2 \cdot \pi \cdot r^2 \cdot dr = 0.616 \cdot \pi \cdot \rho \cdot {R_{disc}}^4 \cdot \left(\frac{\mu}{\rho} \cdot \omega^3\right)^{0.5} \tag{3}$$

$$\rho = \frac{p_{atm}}{287 \cdot T_{air}} \tag{4}$$

$$P_{total} = \left(T_{sensor} + T_{bearings\ friction} + T_{friction\ on\ brake\ disc}\right) \cdot \omega = T_{total} \cdot \omega \tag{5}$$

The velocity of the air flow was measured using a Pitot tube positioned 0.89 m upstream from the turbine. Tests were performed for the blower operating at the frequencies of 19.7, 33.4, 47.0 and 60.6 Hz. For these blower frequencies, the mean velocities measured by the Pitot were 3.70, 6.43, 8.98 and 11.58 m/s with standard deviations of 1.24, 0.72, 0.75 and 0.59% of the mean values. These wind velocity values must be corrected because the presence of the turbine causes an increase in wind velocity in the test section. There are some methods reported by studies on Savonius rotors and the method described by Pope and Harper (1966) is the simplest. This method is given by Eq. (6), in which V_c is the corrected velocity, V_u is the uncorrected velocity, h_r is the height of the turbine, d is the turbine diameter and A_c is the test section area of the channel. However, according to Pope and Harper (1966), this method is recommended for experiments with blockage ratio values up to 7.5%, and in this work this value is 25.9% ($(h_r \cdot d)/A_c$). Maskell (1965) provided another method for the blockage effect correction which is given by Eq. (7), where C_{Du} is the uncorrected drag coefficient of the model, C_{Dc} is the corrected drag coefficient of the model and m is a coefficient obtained experimentally. Alexander and Holownia (1978) conducted a blockage correction study on Savonius turbines similar to the Maskell method and obtained the results shown in Fig. 7. In the same study, Alexander and Holownia performed the validation of blockage corrections in turbines operating with blockage ratios up to 30%. Ross (2010) found that the Maskell method promoted better results for blockage corrections. Akwa et al. (2012b) and Kothe (2016) carried out reviews on these blockage correction methods. Therefore, using the data of Fig. 7, the velocity values of this work were corrected by a factor of 1.3862. Parallel studies on turbine operation without the aerodynamic channel blockage effect have being developed using computational fluid dynamics to validate tests and improve the flow analysis.

$$V_c = V_u \left[1 + \left(\frac{1}{4} \cdot blockage\ ratio\right)\right] = V_u \left[1 + \left(\frac{1}{4} \cdot \frac{h_r \cdot d}{A_c}\right)\right] \tag{6}$$

$$\frac{C_{Du}}{C_{Dc}} = \frac{V_c^2}{V_u^2} = \frac{1}{1 - m \cdot (blockage\ ratio)} = \frac{1}{1 - \frac{m \cdot h_r \cdot d}{A_c}} \tag{7}$$

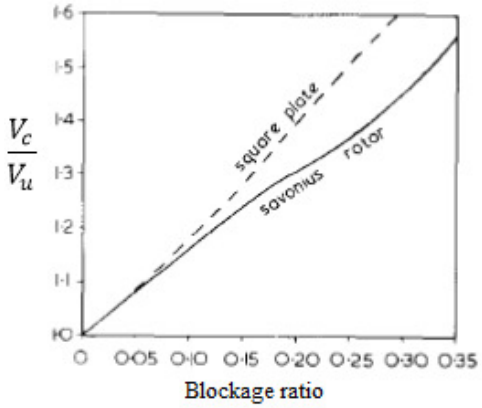

Figure 7 – Correction of the blockage effect presented by Alexander and Holownia (1978).

The Reynolds number values in this study were obtained by taking into account the corrected velocity and the turbine diameter given by Eq. (8). The coefficients of power, C_P, torque, C_T, and tip speed ratio, λ, are obtained by Eq. (9), where r is the radius of the Savonius wind turbine (Akwa et al., 2012b).

$$Re = \frac{\rho \cdot V_c \cdot d}{\mu} \tag{8}$$

$$C_P = \frac{T_{total} \cdot \omega}{\frac{1}{2}\rho \cdot h_r \cdot d \cdot V_c^3} = \left(\frac{T_{total}}{\frac{1}{2}\rho \cdot h_r \cdot d \cdot V_c^2 \cdot r}\right) \cdot \left(\frac{r \cdot \omega}{V_c}\right) = C_T \cdot \lambda \tag{9}$$

3. RESULTS AND DISCUSSION

The main obtained results are curves for the average total torque and power as functions of the angular velocity. The curves were obtained by adjusting the flow in four different average velocity values during the experiments. These curves are show in Fig. 8 and 9 and consistently represent, according to the literature on the subject, the power growth behavior and the torque with increasing wind.

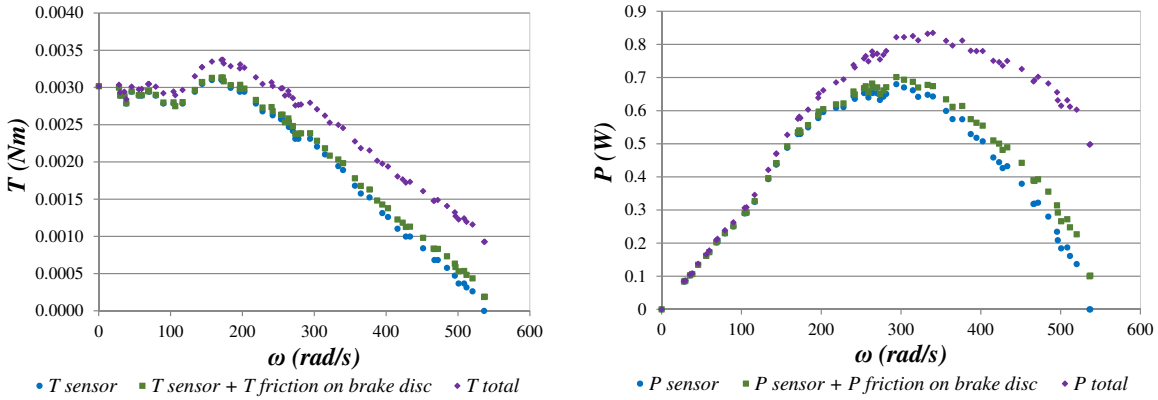

(a) (b)

Figure 8 – Sum of power components in the operation curves for corrected wind velocity 12.45 m/s: (a) torque; (b) power.

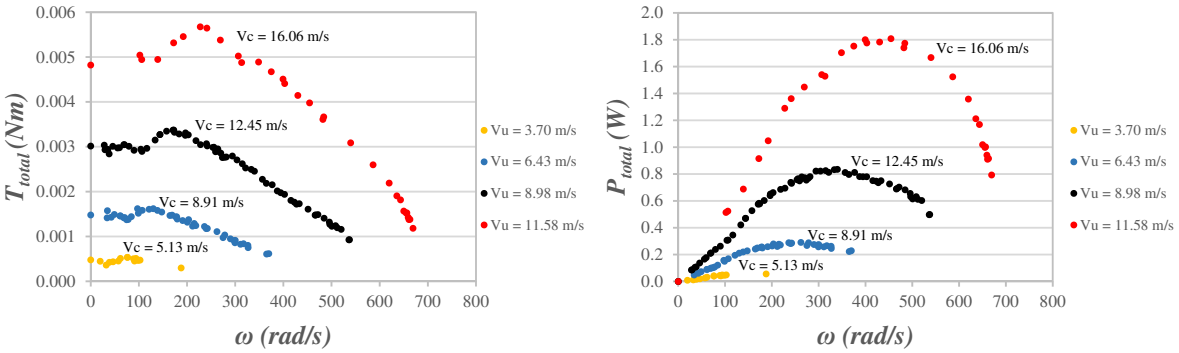

(a) (b)

Figure 9 – Turbine operation curves: (a) mean total torque; (b) mean total power.

The torque and power curves can be dimensionless and transformed into curves of torque and power coefficients in relation to the tip speed ratio of the rotor as shown in Fig. 10. These performance curves are also consistent with values obtained in other studies for this type of turbine, which shows that most Savonius rotor configurations have maximum power coefficients within a broad range, varying from below 0.05 to 0.32 with tip speed ratios around 0.7 (Alexander and Holownia, 1978; Akwa et al., 2012b). The turbine analyzed in this study has only a single stage and did not undergo treatment to reduce surface roughness, which is relatively high for manufacturing with 3D printers. These facts together with the low Reynolds numbers of the flow may have provided a not too high power coefficient value (C_P = 0.107 at λ =

0.707) but it was within the aforementioned range. However, the purpose of this work is to characterize a system for small vertical axis wind turbines by analyzing the operation of the Savonius wind turbine, and this objective was fulfilled.

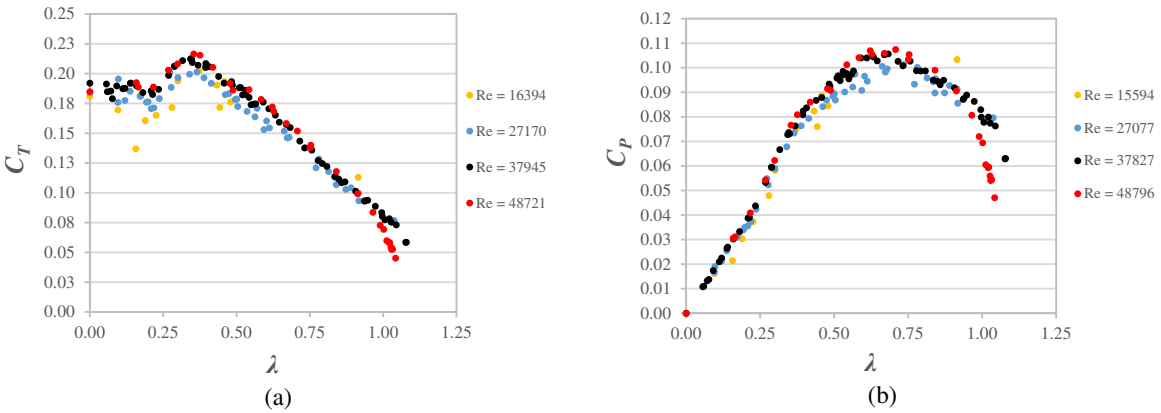

Figure 10 – Turbine performance curves: (a) torque coefficient; (b) power coefficient.

Figure 8 shows the effect of summation of the power that is dissipated due to the friction effect in the bearings and aluminum brake disc with the power measured on shaft by the sensor. Observing this figure, it can be noticed that at the best performance point for operation with corrected wind velocity 12.45 m/s, the angular velocity is 339.92 rad/s and total power is 0.8351 W. At this operation point, the power dissipated by friction in the bearings is 0.1609 W (19.27% of the total) and the dissipated power due the friction in the aluminum brake disc is 0.0311 W (3.72% of the total). Power dissipation by friction tends to increase at high angular velocities and acts to decrease the available power on the turbine shaft. Another friction effect is to slide the power peak to smaller angular velocity values. According to Fig. 8-b the power peak measured by the sensor on the shaft is 0.6800 W at an angular velocity 294.05 rad/s. Thus, the design of small wind turbines should also minimize the bearings friction, without disregarding other constructive and operational parameters.

The maximum power coefficient C_P obtained after the blockage effect correction as shown in Fig. 10-b is 0.107, which occurs at a tip speed ratio of 0.707. At the optimum performance point, the torque coefficient C_T is 0.152, while the maximum torque coefficient is 0.217 in the tip speed ratio of 0.354 (Fig. 10-a). The C_T values grow almost linearly with the decrease of the tip speed ratio λ until the maximum value point and for low λ it remains practically constant with oscillations around a mean value. The C_T and C_P values grow slightly with increasing Reynolds numbers as also explained by Akwa et al. (2012b). However, the curves obtained for the lowest value of Re had greater dispersion in the results because the torque and power values supplied by the turbine were as low as 0.0003 Nm and 0.0286 W making the uncertainty due to the resolution of the sensor more significant.

The values of torque and torque coefficient at the zero angular velocity shown in Fig. 9 and 10 are mean values as functions of the turbine angular position. The static values of C_T measured for 16 turbine angular positions θ are shown in Fig. 11. According to Fig. 11, the torque cycle repeats every 180° because the turbine has 2 buckets. The highest static torque coefficient occurs from 22.5° to 67.5°, while the lowest value occurs around 157.5°. According to Vance (1973) and Akwa et al. (2012b) the 0° position (equal to 180° for a 2-bucket Savonius turbine) does not produce the smallest torque. This is due to the participation of the lift forces in the composition of the resulting forces in the buckets.

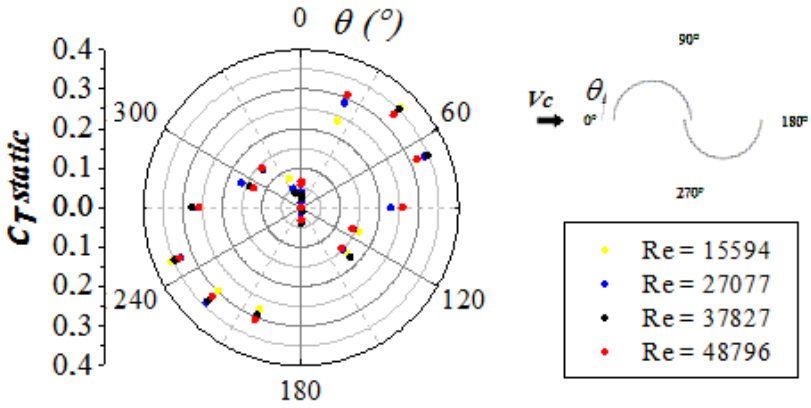

Figure 11 – Static torque coefficient *versus* angular position.

4. CONCLUSION

In the present work, the construction and operation of a small aerodynamic channel were performed allowing the development of a system for the characterization of a vertical axis wind turbine in small scale. In the same way, measurements were made through the aforementioned methodology, obtaining consistent results with the literature on this subject, as the turbine operation curves were given by power, torque and performance coefficients curves.

Some additional tests can still be performed, such as instantaneous angular velocity measurements by means of the encoder and studies on the turbine operation without the aerodynamic channel blockage effect. These last analyses are being developed at the laboratory using computational fluid dynamics in validation tests and flow analysis. Thus, the system can be used in the future to test different configurations of small vertical wind turbines with low cost and space saving at Renewable Energy Laboratories.

5. ACKNOWLEDGEMENTS

The authors thank the financial support from São Paulo Research Foundation (FAPESP) to the research project (grant n. 2017/16766-3). The authors also thank the financial support from CAPES through the scholarship to G. D. Barbosa (Finance Code 001).

6. REFERENCES

Akwa, J. V.; Alves da Silva Júnior, G.; Petry, A. P., 2012a. “Discussion on the verification of the overlap ratio influence on performance coefficients of a Savonius wind rotor using computational fluid dynamics". *Renewable Energy*, Vol. 38, pp. 141–149.

Akwa, J. V.; Vielmo, H. A.; Petry, A. P., 2012b. "A review on the performance of Savonius wind turbines”. *Renewable and Sustainable Energy Reviews*, Vol. 16, pp. 3054–3064.

Akwa, J. V., 2014. *Estudo Numérico e Experimental do Escoamento Sobre um Rotor Eólico Savonius em Canal Aerodinâmico com Alta Razão de Bloqueio*. Tese de Doutorado, Universidade Federal do Rio Grande do Sul, Porto Alegre, Brasil.

Alexander, A. J.; Holownia, B. P., 1978. “Wind Tunnel Tests on a Savonius Rotor”. *Journal of Industrial Aerodynamics*, Vol. 3, No. 4, pp. 343–351.

Fujisawa, N., 1992. “On the Torque Mechanism of Savonius Rotors”. *Journal of Wind Engineering and Industrial Aerodynamics*, Vol. 40, No. 3, pp. 277–292.

Lopes, W., 2008. “Variação da Aceleração da Gravidade com a Latitude e Altitude”. *Caderno Brasileiro de Ensino de Física*, Vol. 25, No. 3, pp. 561–568.

Kamoji, M. A.; Kedare, S. B.; Prabhu, S. V., 2008. “Experimental Investigations on the Effect of Overlap Ratio and Blade Edge Conditions on the Performance of Conventional Savonius Rotor”. *Wind Engineering*, Vol. 32, No. 2, pp. 163–178.

Kothe, L. B., 2016. *Estudo Comparativo Experimental e Numérico sobre o Desempenho de Turbinas Savonius Helicoidal e de Duplo Estágio*. Dissertação de Mestrado, Universidade Federal do Rio Grande do Sul, Porto Alegre, Brasil.

Kumar, R.; Raahemifar, K.; Fung, A. S., 2018. “A critical review of vertical axis wind turbines for urban applications”. *Renewable and Sustainable Energy Reviews*, Vol. 89, pp. 281–291.

MacPhee, D. W.; Beyene, A., 2019. “Performance analysis of a small wind turbine equipped with flexible blades”. *Renewable Energy*, Vol.132, pp. 497–508.

Menet, J. L., 2004. “A Double-step Savonius Rotor for Local Production of Electricity: a Design Study”. *Renewable Energy*, Vol. 29, pp. 1843–1862.

Pope, A. and Harper, J., 1996. *Low Speed Wind Tunnel Testing*. John Wiley & Sons, New York.

Rosa, E. S., 2009. “Disco Rotativo de Von Kármán, in: Camada Limite Tri-Dimensional, apostila de material didático de disciplina de mecânica dos fluidos” Faculdade de Engenharia Mecânica da UNICAMP. 10 Jan. 2019 <http://www.fem.unicamp.br/~im250/APOSTILAS%20E%20MINI-CURSOS/EQ3DCL_tudo.pdf >.

Ross, I. J., 2010. *Wind Tunnel Blockage Corrections: An Application to Vertical-Axis Wind Turbines*. Master thesis, University of Dayton, Dayton, Ohio, USA.

Saha, U. K.; Thotla, S.; Maity, D., 2008. “Optimum Design Configuration of Savonius Rotor through Wind Tunnel Experiments”. *Journal of Wind Engineering and Industrial Aerodynamics*, Vol. 96, pp. 1359–1375.

Streeter, V. L., 1974. *Mecânica dos Fluidos*. Editora McGraw-Hill do Brasil, São Paulo.

Savonius, S. J., 1930. *Wind Rotor – Patent 1,766,765*. United States Patent Office.

Van Wylen, G. J.; Sonntag, R. E.; Borgnakke, C., 1995. *Fundamentos da termodinâmica clássica*. Editora Blucher, São Paulo, translation of the 4th edition published in the USA by John Wiley & Sons.

Vance, W., 1973. “Vertical Axis Wind Rotors – Status and Potential”. In *Proceedings of the Conference on Wind Energy Conversion Systems.* Washington, USA, pp. 96-102.

Maskell, E. C., 1965. *A Theory of the Blockage Effects on Bluff Bodies and Stalled Wings in a Closed Wind Tunnel*. Aeronautical Research Council Reports and Memoranda, London.

7. RESPONSIBILITY NOTICE

The authors are the only responsible for the printed material included in this paper.